

‘Bionic skin’

Igor Kovalev

Kinneret College on the Sea of Galilee, Emek Hayarden 15132, Israel

kovis@ashdot-m.org.il

Abstract: The lift force and vibration performance of a NACA-230 airfoil with a ‘bionic skin’ (metallic version of the butterfly scale) were experimentally investigated. Attention was initially directed to this problem by studies indicating a better lift, maneuver, vibration and noise performance of flying butterflies, covered with scales. Results indicated that the ‘bionic skin’ of an oscillating rotor blade increased the lift force by a factor of 1.15, reduced both the damping coefficients by a factor of 1.23, and the vibration by a factor of 1.17. The modification of the aerodynamic effects on the rotor blade was due to an increase of the virtual air mass, which influenced the ‘bionic skin’. The air cavity of the skin increased the virtual air mass by a factor of 1.2. The interaction mechanism of a ‘bionic skin’ with a flow and a sound wave was described. [Researcher. 2010;2(9):41-49]. (ISSN: 1553-9865).

Keywords: bionic, blade, butterfly, helicopter, lift, noise, skin, vibration, virtual mass.

Nomenclature

A.C.	air cavity
B.S.	‘bionic skin’
CRE	closed root edge
d.s.	downstream
E	Young’s modulus
F	aerodynamic loading / lift force
f	oscillation frequency
HP	high pressure
I_x	second moment
k	stiffness of blade
l	beam length
L.A.	longitudinal axis
LE	leading edge
LL	lower lamina
LP	low pressure
L.W.	lower wall
m	total mass of the flapping blades
m_m	oscillating blade mass
m_v	virtual air mass
n	cycle number
q	amplitude oscillation / tip deflection / peak magnitude of a cycle
P	perforations
R	riblets
R.B.	rotor blade
S.G.	strain gauges
T	trabecula
t	time
t_t	beam thickness
TiE	tip edge
TrE	trailing edge
UL	upper lamina
u.s.	upstream
W	sound wave
w	beam width
ξ	damping ratio
ξ_1	damping ratio of the rotor blade with the smooth skin

- ξ_2 damping ratio of the rotor blade with the ‘bionic skin’
- δ logarithmic decrement
- δ_1 logarithmic decrement of the rotor blade with the smooth skin
- δ_2 logarithmic decrement of the rotor blade with the ‘bionic skin’
- 1 mean flow/ fluid flow
- 2 aspiration of air
- 3 secondary flow
- 4 discharge of air

1 Introduction

1.1 Butterfly scales

The surface of the wings of present day butterflies is covered with millions of tiny appendages – scales (30-200 μm in size). Each butterfly scale is a long and flattened extension of cuticle and generally resembles a gathered sack consisting of lower and upper laminae (Figure 1) [Weber, 1933]. These laminae are separated by a hollow region. The lower lamina is a flat plate from which trabeculae rise to join the upper lamina. The upper lamina is a complex structure consisting of ridges (spacing 2 μm) with an inverted V-profile and grooves which discrete openings. The inverted V-profile of the ridges form the micro channels (1.5 - 2 μm in clear lamina spacing), which are disposed between the airpermeable upper laminae and airproof lower laminae. The root edge of the wing scale is closed, and the tip edge is open.

There are some peculiarities with butterflies: they are the youngest insects in terms of their evolutionary history. The ancestors of present day butterflies flitted into air about 200 million years ago. Through natural selection, the butterflies have been

experimenting with scale microstructure and scale coverage for two hundred million years. Among all present day insects, butterflies and moths with scale coverage are the record holders of two titles: long distance travel (butterfly *Danaus plexippus L.*) and flight speed (moth *Macroglossum stellatarum L.*) [Demoll, 1918].

Scale microstructure and scale coverage of present day butterflies are multifunctional. Laboratory examinations showed that the presence of the scales minimized the vibration of the butterfly *Vanessa urticae L.* [Kovalev and Brodsky, 1996], decreased the noise produced by the flying moth *Barathra brassicae L.* [Kovalev, 2003], and absorbed the ultrasonic squeaks produced by bats (moth *Gastropacha populifolia esper*) [Kovalev, 2004]. Moreover, a scale coverage increased the lift of fixed-wings of the nocturnal moth (*Catoealer*) [Nachtigall, 1974], and extended the movement capability (maneuverability) of the flying moth *Tinea tapotialla L.* (Figure 2). This property of the scales allows the butterflies to overcome the predator attacks in the sky.

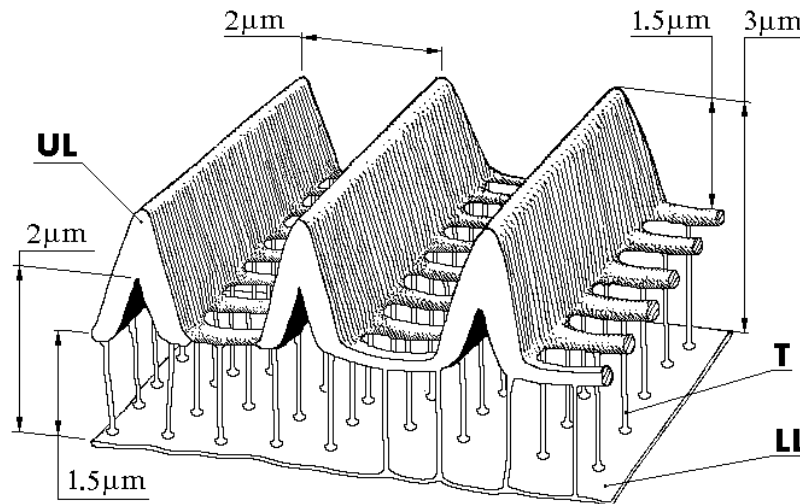


Figure 1. A vertical cross-section of *Pyrameis atalanta (L)* butterfly wing scale. UL – upper lamina, LL – lower lamina, T – trabecula.

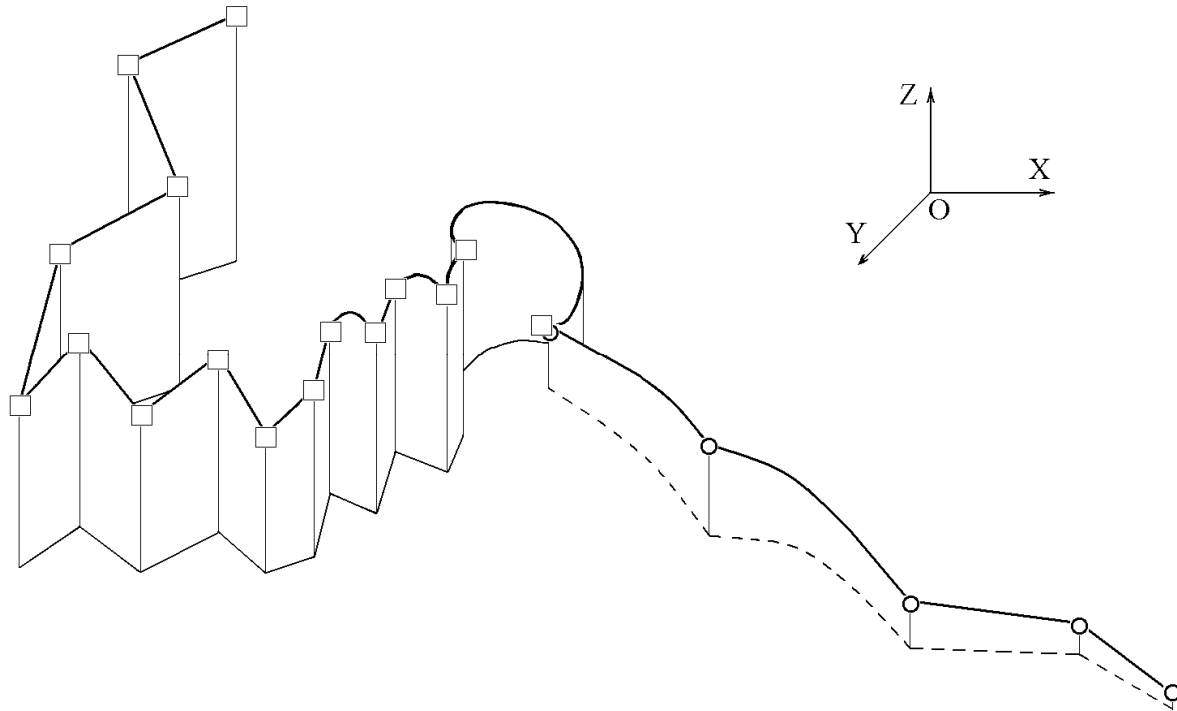


Figure 2. Flight trajectories of the moth *Tinea tapotiella* L. in take – of flight. The flight trajectories of the moth with scale coverage and without it are expressed by lines with open squares and open circles, respectively, and the flight trajectories projected onto the plane XOY by the solid and dotted lines, respectively. The time of the flight was 5 second.

1.2 Helicopter

A history of helicopter development is usually begun with mention of Paul Corny (France, 1907). He constructed a machine that made the first flight with a pilot (Corny). This helicopter achieved an altitude of about 0.3 m for 20 sec. The initial development of rotary-wing aircraft faced three major problems which limit the forward speed of a helicopter, and reduce maneuvering capability of an aircraft. The first problem was to develop a light and strong structure for rotor blades while maintaining good aerodynamic efficiency. The second problem was to design the quiet helicopter, and the final problem was to minimize the vibration of the helicopter [Johnson W., 1980]. In order to eliminate the problems of rotor blades of helicopter, I studied the influence of ‘bionic skin’ (metallic version of the butterfly scale) on the rotor performance.

2 Material and method

2.1 Wind-tunnel

The aerodynamic properties of rotor blades were tested in a small open-jet wind-tunnel. Air was driven by a fan (diameter of 30 cm) into a wide

chamber (diameter of 1000 cm) where its velocity was low. The screen of wire gauze helped to equalize the velocity, where across the cross-section of the chamber. The honeycomb ensured that there was no large-scale swirling around in the channel, but that the air traveled along it in straight lines. The irregularity of wind of the wide chamber was swamped by the large space. Thus the uniform increase of velocity that occurred when the air passed through the much narrower nozzle (25cm x 50 cm in size). The contraction section of the nozzle was designed using a matched pair of cubic curves. Thus, the wind in the working section was uniform and laminar. The air speed of the wind tunnel was 50 m/s. One typical Reynolds based on chord length on this wind speed was 330000.

The wind in the test section was measured using a Pitot-static tube connected to a Datametric Barocel Electronic Manometer. Pressure difference down to 0.0001 in H₂O could then be measured. Turbulent velocity data and mean speed were also measured by using a constant temperature hot-wire anemometer. The temperature of the air was maintained at 20°C.

2.2 Rotor blades

Two different rotor blades were used. The skin of the first rotor blade (Figure 3) was obtained from the *Pyrameis atalanta* (*L.*) wing scale (Figure 1), and the skin was 333 times life size (the thickness was 1 mm) (Figure 3). This skin, called ‘bionic skin’, was composed of two layers. The upper metal wall and the lower metal wall were separated by an air cavity (from 0.4 to 0.7 mm in clear spacing). Both sides of the upper wall were covered with a large number of chordwise grooves. The depth of each groove was 0.5 mm. The ridges (spacing 1 mm) with an inverted V-profile were formed between grooves. The grooves of the external surface were provided with lines of perforations (each opening was 0.4 mm

x 0.4 mm in size). The inverted V-profile of the ridges formed the channels, which were disposed between the upper metal wall and lower wall. The lower metal wall was similar to a thin sheet.

The second rotor blade was geometrically similar to the first wing (the blade airfoil was NACA 230; the chord of the wings was 10 cm and the length was 25 cm). It was the principal concern of this study to qualitatively determine the effect of ‘bionic skin’ on aerodynamic forces of an oscillating wing. Therefore, the skin of the second rotor blade was mono-layered, smooth and airproof. The design of the skin is traditional for modern helicopters. The aerodynamic properties of the first rotor blade were compared with those of the second rotor blade.

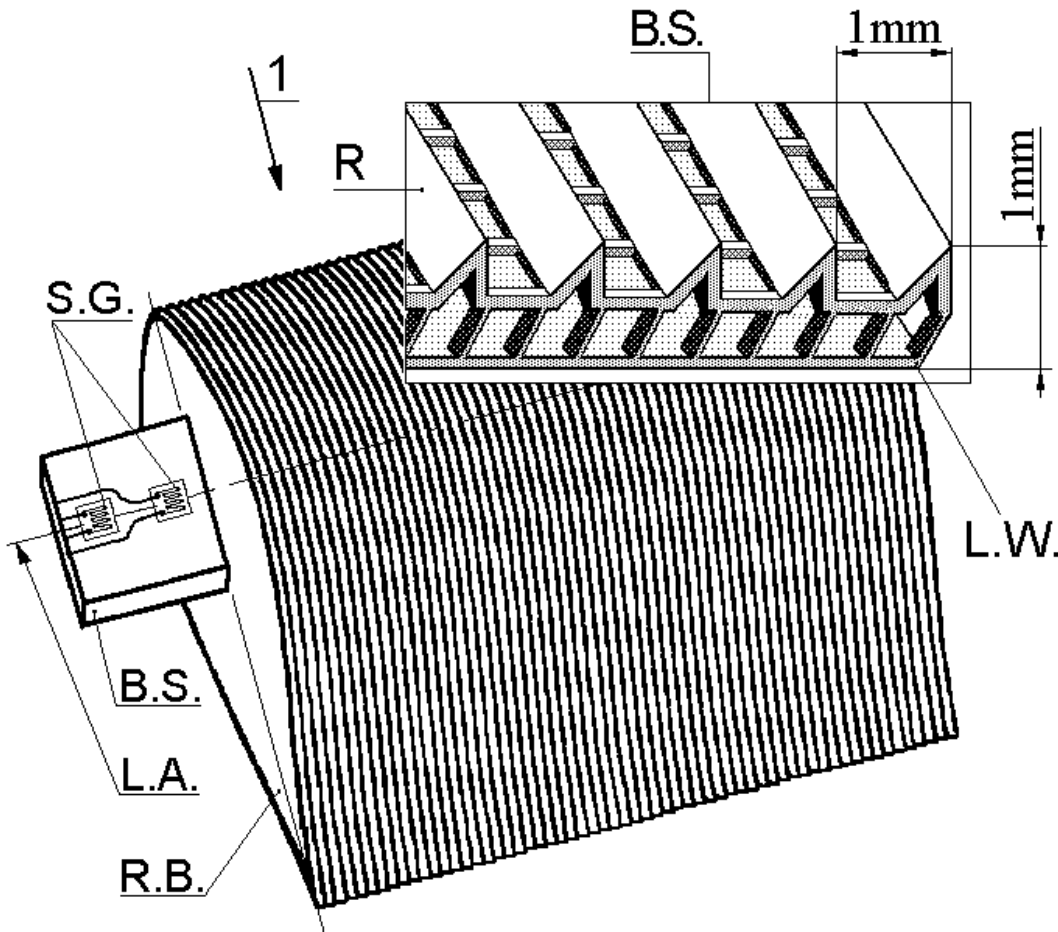


Figure 3. A rotor blade with the ‘bionic skin’.

1 – mean flow; L.W. - lower wall; B.S. - ‘bionic skin’; R - riblets (grooves); B.S. – beam spring; R.B. – rotor blade; L.A. – longitudinal axis, S.G. - strain gauges.

2.3 Force measurement

The forces on the rotor blades were measured using a force balance. The balance was designed for a measurement range between 0.1 mm and 10 mm amplitude of flapping motion of tip edge. The calibration accuracy and the resolution at low speeds was ± 0.1 mm amplitude. The suspension of the balance was the beam spring (Figure 3). The width of the beam spring was 30mm and the thickness was 5 mm. Four strain gauges (Figure 3) (gauge type CEA-13-125 UW-120) were mounted on both sides of the beam spring. Each force sensing element was attached to the longitudinal axis (Figure 3) of the suspension of the balance. Two orthogonally pairs of the transducers were wired in full bridge configuration. The sensitivity of the transducer with 10 V excitation were 700 NV^{-1} and 740 NV^{-1} . The load sensitivity of the balance was adjusted by an exchangeable beam spring. Each rotor blade was fixed to the suspension of the force balance so that a transducer channel measured the forces perpendicular to the chord plane. These forces were then used to calculate the lift.

3 Result and discussion

3.1 Unsteady Aerodynamic loading

Rapidly increasing the angle – of – attack of rotor blades in the flow triggered flapping motion. The frequency of the rotor blade with the ‘bionic skin’ was 2.9 Hz, and the frequency of the rotor blade with the smooth skin was 3.4 Hz (Figure 4). This result showed that the ‘bionic skin’ reduced the vibration of the rotor blade by a factor of 1.17. The following sequence of unsteady environment events in both the first rotor blade and the second rotor blade was observed at high rates of angle – of – attack change: initially an overshoot of loading; then a decrease of the aerodynamic loading; and finally, a steady aerodynamic environment of the rotor blades. As shown in Figure 4 that an aerodynamic influence on the rotor blades in unsteady conditions was far more powerful than in static conditions. The character of the unsteady aerodynamic loading on the rotor blades compares well with one on an airfoil for high rates of angle – of – attack change [Ham and Garlick, 1968].

As shown in Figure 3, the rotor blade, which is fixed on the beam spring, is not beams of regular cross section. Experimental tests with fixed wing on a beam spring, which was loaded as cantilevers, revealed that this construction would behave as was predicted by simple beam – bending theory [Ham and Garlick, 1968]. Therefore, I assumed that the rotor blades in flow would behave like cantilevered beams of regular cross section (the width of the beams $w =$

30 mm, the thickness $t_t = 5$ mm), which were loaded by air force F .

The following relationships were used to compute the aerodynamic loading F of the two flapping blades.

$$F = 3EI_x q/l^3, \quad (1)$$

where E is Young’s modulus, $E = 2 \times 10^{11} \text{ N m}^{-2}$; q is amplitude of oscillation, or tip deflection; l is length of beam, $l = 270$ mm for the two models; I_x is second moment of cross section area given by

$$I_x = wt_t^3/12. \quad (2)$$

The calculation shows that the ‘bionic skin’ of the rotor blade increases the aerodynamic loading F by a factor of 1.15. This result is in good agreement with the experimental data of the lift given by Nachtigall for a moth wing with scales [Nachtigall, 1974]. Moreover, aerodynamic influence on the rotor blade with the ‘bionic skin’ in unsteady conditions was more lasting than on the rotor blade with the smooth skin.

3.2 Damping coefficients

Damping is the process by which vibration steadily decreases its amplitude. The rate at which the vibration amplitude decays is controlled by the damping ratio ξ . The damping ratio ξ may be determined by:

$$\xi = \frac{\delta}{\sqrt{\delta^2 + 4\pi^2}} \quad (3)$$

The logarithmic decrement of δ were obtained by:

$$\delta = \frac{1}{n} \ln \frac{q_0}{q_n}, \quad (4)$$

where n is the cycle number, q is the peak magnitude of this cycle (Figure 4). The analysis of the oscillogram shows that the damping ratio of the rotor blade with the ‘bionic skin’ was $\xi_2 = 0.058$, and one of the rotor blade with the smooth skin was $\xi_1 = 0.07$; the logarithmic decrement of the first rotor blade was $\delta_2 = 0.36$, and one of the second rotor blade was $\delta_1 = 0.44$. The calculation ξ_2 and δ_2 is based on peak magnitudes of amplitudes q_0 and q_4 ; the calculation ξ_1 and δ_1 is based on peak magnitudes of amplitudes q_0 and q_5 (Figure 4). We thus see that the ‘bionic skin’ reduces the damping ratio ξ of the flapping rotor blade by a factor of 1.23. This result shows that the first rotor blade is less damping than the second rotor blade. The damping of the blades oscillation in air flow has two sources. There is damping due to

internal rope friction, and there is also aerodynamic friction on the rotor blade. Since in this experiment the internal rope friction is identical for both first and second blade, it follows that the damping reduction of first blade oscillation is due to an aerodynamic

friction reduction. A drag reduction capability of the 'bionic skin' is consistent with results from studies of an artificial surface of shark scales [Becher et al., 1985].

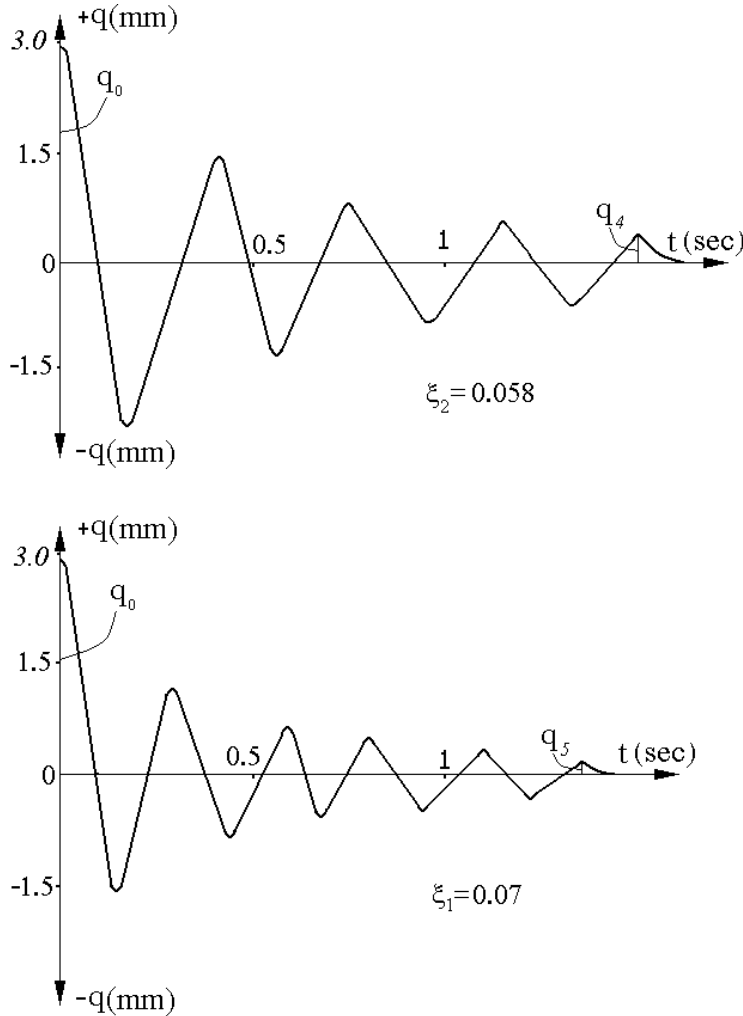


Figure 4. Upper oscillogram is the flapping motion of the rotor blade with the 'bionic skin'. Lower oscillogram is the flapping motion of the rotor blade with the smooth skin.

q – amplitude, t – time, ξ –damping ratio.

3.3 Virtual air mass of oscillation blades

The analysis of Figure 4 shows that a 'bionic skin' reduces the frequency by 8% (as described above). The oscillation frequency f may be determined as follow:

$$f^2 = k/m, \tag{5}$$

where k is the stiffness of blade

$$k = 3EI_x/l^3. \tag{6}$$

m is the total mass of the flapping blades

$$m = m_m + m_v, \tag{7}$$

where m_m is the oscillating blade mass; m_v – virtual air mass. Since the first and the second blades were subjected to the flow at identical model mass m_m and stiffness of model k , it follows that the reduction of the frequency of the

rotor blade with the 'bionic skin' f was a result of an increase of the virtual air mass m_v , which influences the wing and is set in motion together with the oscillating blade. Using the expressions for the frequency f (5) and the total mass m (7), we find that the 'bionic skin' increases the air mass which influences the blade by a factor of 1.2.

3.4 The concept of the flow and 'bionic skin' interaction

Bechert described the interaction mechanism of shark skin with a turbulent boundary layer [Bechert et al., 1985]. Savill developed the interaction mechanism of a hollow construction wall with a sound wave [Savill, 1993]. I developed the interaction mechanism of a 'bionic skin' with a flow and a sound wave on a basis of Bechert's and of Savill's mechanism. Figures 5 and 6 show schematic drawing what can be assumed to happen.

3.4.1 An increase in the lift force

In Figure 5 I plotted a local flow pattern in Y-Z-X – plane around a cross-section of the 'bionic skin'. The rapidly raised angle – of- attack of helicopter rotor with butterfly skin produces a region of high pressure of air HP on the upper wall surface facing the mean flow 1 (Figure 5). In this region, air is released downward perpendicularly through the holes of the perforated wall into the region of low pressure LP of the air cavity. The aspiration of the air 2 (Figure 5) in the recess produces both a pressure increase in the cavity and the air transfer 3 in a direction from the closed root edge CRE to the nozzle of the tip edge TiE. The inverted V - profile of the ridges forms the channels between the upper and lower walls. These channels as well as the ridges determine a direction both of secondary flow 3 and of the discharge of air 4 from the skin nozzle (Figure 5). The comparison of the interaction mechanisms of the two wings show that the rotor blade with the 'bionic skin' interacts with mean flow 1, enter flow 2, pass flow 4, and second flow 3. On the other hand the no cavity skin interacts only with mean flow. Thus the structure of butterfly skin increases the volume of the virtual air which influences the rotor blade.

Inviscid flow theory shows that aerodynamic forces are proportional to the volume of the virtual air which influences the wing surface, i.e. the larger volume of the virtual air, the more aerodynamic forces of the rotor is needed. The 'bionic skin' increases the volume of the virtual air (as described above), hence the skin increases the lift force of rotor.

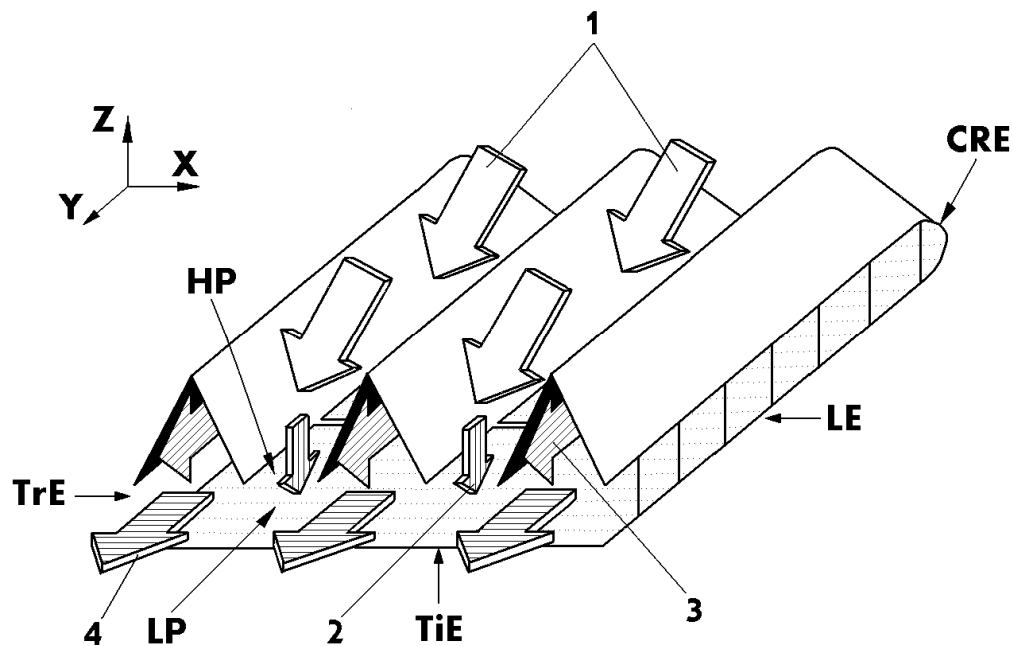


Figure 5. The influence of the flows on the surface configurations of 'bionic skin'.

1 – mean flow; 2 – aspiration of air; 3 – secondary flow; 4 – discharge of air; HP - high pressure; LP - low pressure; CRE – closed root edge; TiE - tip edge; TrE – trailing edge; LE – leading edge.

3.4.2 An aerodynamic friction reduction

It is well known that the same pressure difference is present in a turbulent flow over an outer surface of a flapping wing [Johnson, 1980]. In this experiment the reduction of the flow resistance is probably a result of different pressure compensation of the airflow by the air cavity of 'bionic skin'. If a region of low pressure is involved on the upper wall surface, fluid from the air cavity will pass out into the surroundings. If a region of high pressure is involved on the upper wall surface, fluid will enter the air cavity from the mean flow. This mechanism appears likely to decrease the magnitude of the pressure fluctuations, and to reduce the drag caused by friction airflow over the flapping blade.

3.4.3 Decrease the noise and the vibration

The contributions to helicopter rotor noise can be classified as blade slap and rotational noise. Blade slap is produced by the periodic lift acting on the blade, which result in impulsive sound wave W radiation (Figure 6). The wave W produces change, with higher pressure downstream $d.s.$ of the slap and the air cavity Re form a plenum through which air is transferred in a direction counter to the air flow 1 from the higher pressure region downstream $d.s.$ of the slap to the lower pressure upstream $u.s.$ of the slap. The permitting recirculation of boundary layer air in this manner is known for the reduction of slap effect, in particular the pressure drag. The principal source of rotational noise is boundary layer turbulence. It is known that any improvement in aerodynamic efficiency the rotor can be reduced both the helicopter rotor noise and vibration, which are transmitted to the fuselage. The 'bionic skin' improves the boundary layer flow (as described above), hence reduces both the rotational noise and vibration.

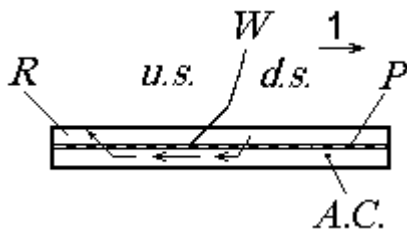


Figure: 6 An axial section of 'bionic skin' in a fluid flow in which there is a sound wave W .
 P - perforations; 1 - fluid flow; $u.s.$ - upstream; $d.s.$ - downstream; R - riblets; $A.C.$ - air cavity; W - sound wave.

In steady-state forward flight, the periodic forces at the blade are transmitted to the helicopter airframe, producing a periodic vibratory response. 'Bionic skin' structure minimizes the helicopter vibrations by aspiration of air into the air cavity, drawing air in the recess and returning into the surroundings. The energy of the transmitted vibration thus in highly dissipated into the 'bionic skin'.

Summary

It thus seems that the helicopter rotor with the 'bionic skin' has, at Reynolds numbers 330000, the obvious advantages of lift, low vibration and low aerodynamic friction reduction by comparison with the traditional rotor blade. The modification of the aerodynamic effects on the rotor is due to an increase in the virtual air mass, which influences the 'bionic skin' and is set in motion together with the oscillation wing. It is conceivable that increasing the clear layer spacing of air cavity would tend to increase the virtual air volume even more. However, a parametric study of a hollow region was not within the scope of this experiment. A full explanation must await more detailed studies, but it does not seem unreasonable to suggest the possibility of some optimal cavity geometry to further augment the lift and to reduce the aerodynamic friction.

It is evidently, that higher performance of helicopter rotor with the 'bionic skin' will ensure outstanding flying quality, safety, and comfort of aircraft.

Acknowledgements

I would like to thank my advisor Dr. Olga Bocharova – Messner for her ideas and comments. Her input has contributed significantly to this work. I thank external reviewers for their constructive comments.

References

1. Bechert, D.W., Hoppe G., and Reif W. - E., 1985, On the drag reduction of the shark skin,
2. American Institute of Aeronautics and Astronautics, Paper No 85 - 0546, March 12 - 14, 18p.
3. Demoll, R., 1918, Der Flug der Insekten und der Vogel, Gustav Fischer, Jena.
4. Ham, N.D., Garelick M., 1968, "Dynamic Stall Considerations in Helicopter Rotors," Journal of the American Helicopter Society, April 13, p. 49.
5. Johnson W., 1980, Helicopter Theory. Princeton University Press, 1024.
6. Kovalev I.S., Brodsky A.K. 1996, Of the role that elasticity and scales coating of the

- wings play in the flight stability of insects. Bulletin of the S. Petersburg State University, series 3, issue 3, p. 3-7.
7. Kovalev I.S. 2003, Acoustic properties of wing scaling in Noctuid Moth. Entomological Review, v. 82, issue 2, 270-275 p.
 8. Kovalev, I.S., 2004, Effect of the scales coverage of the moth *Gastropacha populifolia* *esper* (*Lepidoptera, lasiocampidae*) on the reflection of the bat echolocation signal, Entomological Review, Vol. 83, No. 3, pp. 513 - 515.
 9. Nachtigall W., 1965, Die aerodynamische Funktion der Schmetterlingsschuppen // Naturwissenschaften, Bd 52, H.9, S. 216 - 217.
 10. Savill A.M., 1993, Control of fluid flow, Patent # WO 93/19980.
 11. Weber H., 1933, Lehrbuch der entomologie, Veslag Gustav Fischer, Jena, Germany, 728 p.

4/15/2009